Learning and Nonlinear Models - Journal of the Brazilian Society on Computational Intelligence (SBIC), Vol. 21, Iss. 1, pp. 47-59, 2023

Fuzzy control of a high-performance boost converter in discontinuous conduction mode and its application to a photovoltaic pumping system

Igor R. Sousa
Graduate Program on Teleinformatics Engineering - Federal University of Ceará (UFC)
Center of Technology, Campus of Pici, Fortaleza, Ceará, Brazil
igor.sousa@alu.ufc.br

Cláudio M. S. Medeiros
Graduate Program on Renewable Energy - Federal Institute of Ceará (IFCE)
Campus of Maracanaú, Maracanaú, Ceará, Brazil
claudiosa@ifce.edu.br

Guilherme A. Barreto
Graduate Program on Teleinformatics Engineering - Federal University of Ceará (UFC)
Center of Technology, Campus of Pici, Fortaleza, Ceará, Brazil
gbarreto@ufc.br

Abstract – In this work, a fuzzy voltage controller design of a 1 kW high-gain, high-efficiency direct current converter operating in discontinuous conduction mode is developed. In this condition, the design of a conventional controller is more challenging. This converter is part of an autonomous photovoltaic pumping system without batteries consisting of four photovoltaic modules, a variable frequency inverter and an induction motor coupled to a pump. The boost converter is responsible for the voltage elevation of photovoltaic modules to a 311V direct current bus, which must not have oscillations for a good operation of an algorithm to track the maximum power point of the modules. The fuzzy controller was implemented in a digital signal processor device to control the boost converter, producing a response with an overshoot of $5.78\,\%$, settling time of $3.8\,s$ and zero error in steady state.

Keywords – Photovoltaic pumping, fuzzy control, boost converter.

1. INTRODUCTION

Photovoltaic pumping systems are generally composed of a set of photovoltaic panels, a direct current (DC) bus and an electronic converter to drive the motor-pump set. To drive a $220\,V$ induction motor, the DC link needs a voltage of $311\,V$. The need to use many photovoltaic panels in series to reach this voltage, as in Raju, Kanik and Jyoti [1], makes many authors use a DC-DC boost converter, obtaining the desired voltage with fewer panels. We can also highlight the work of Vongmanee [2], who used a classic DC-DC boost converter. However, the gain of this converter is limited by the switching losses in the transistor, diode and series resistance of the capacitor and inductor [3].

Ferreira Filho *et al.* [4] use a high voltage gain DC-DC boost converter based on the three-state switching cell (HVG-TSSC) proposed by Torrico-Bascopé *et al.* [5]. One of the main advantages of this converter is that the low blocking voltages in the switches allow the use of low resistance MOSFETs, increasing the converter efficiency. A high performance and a high static gain make this converter a very attractive option for use with few photovoltaic panels in series [5]. Ferreira Filho *et al.* [4] and Silveira *et al.* [6] report an efficiency of this converter above 93%, for a prototype with a power of $1\,kW$.

In order to keep the output voltage of the boost converter constant independently of moderate variations in the input voltage, it is common to implement a voltage control loop with linear controllers, either based on conventional structures [7] or on state feedback [8]. For the design of these controllers, it is necessary to create a linear model to dynamically represent the boost converter. One option is to formulate a transfer function model based on small signal theory [9]. However, in some cases, especially when faced with strong nonlinearities, the application of this technique still does not provide a satisfactorily representative model of the problem. Thus, the application of nonlinear controllers based on the empirical knowledge of experts, such as fuzzy controllers, becomes an appealing alternative. Fuzzy logic is widely used in power system stabilization, as in Eltag and Aslamx [10].

In the control system proposed by Ferreira Filho *et al.* [4], the authors use a conventional digital PI-type (Proportional Integral) controller to control the output voltage of the DC-DC HVG-TSSC boost converter, designed by Silveira and Torrico-Bascopé [6]. In this case, the authors operate the converter only in continuous conduction mode, which facilitates the elaboration of a linear model.

In the application discussed in the current article, the authors are faced with the operation of the DC-DC HVG-TSSC boost converter in the discontinuous conduction mode (DCM). This conduction mode appears during the initialization process of the

photovoltaic pumping system, during times of low irradiance or lack of water for pumping. The operation of the DC-DC HVG-TSSC boost converter in DCM without a specific control for this mode can induce problems in other stages of the photovoltaic pumping system, such as voltage oscillations that hinder a good maximum power point tracking (MPPT) of photovoltaic panels. Other fuzzy controllers for classic boost converters, as in [11], should not be used in the DC-DC HVG-TSSC boost converter because they have different topologies, and mainly because, in this specific case, they work in different conduction modes.

This work deals only with the output voltage control of a DC-DC HVG-TSSC boost converter in DCM that integrates a photovoltaic pumping system. A Mamdani-type fuzzy inference system is used as controller and is compared with the performance of state feedback controller and classic PI controller for continuous conduction mode proposed by Ferreira Filho *et al.* [4].

The organization of this work is as follows. Section 2 presents the real plant of control to be used in this work. Section 3 contains information about the DC-DC HVG-TSSC boost converter and explanations why conventional controllers are not a good solution to the problem. Section 4 deals with the state feedback control technique. Section 5 deals with the fuzzy controller project for the problem. The section 6 presents the simulation results and real results of the control system. Finally, Section 7 describes the work's conclusions.

2 VOLTAGE CONTROL SYSTEM

The system input consists of four CS6K-270 photovoltaic panels from *Canadian Solar*®. The association of the four panels is done as follows: two panels are connected in series and they are in parallel with two other panels in series. Blocking diodes are used to avoid problems related to voltage mismatch. The four panels are placed side by side and can be seen in Figure 1a.

The DC-DC HVG-TSSC boost converter to be used is responsible for the voltage elevation of the panels to $311\,V$ of the DC bus of the pumping system. The converter was built by the Energy Processing Laboratory research group of the Federal Institute of Science, Education and Technology of Ceará (*IFCE*), Fortaleza, Ceará, Brazil. The pulse width modulation (PWM) signals from the DSP for the boost converter command are connected to the MC33152p driver.

The electronic system built for this work, based on the converter proposed in [6], is shown in Figure 1b. This figure shows the board with the DSP, the DC-DC boost converter and the input of the photovoltaic panels. The auxiliary power supply in the figure powers the driver circuit of the DC-DC HVG-TSSC boost converter and the DSP microcontroller from the panels.

To control the output voltage of the DC-DC HVG-TSSC boost converter, the Texas® DSP TMS320F2812 is used. The main characteristics of this DSP that led to its choice for this work are the following: 150MHz clock frequency, 16 analog ports multiplexed in two 12-bit A/D converters, two independent event handlers, 32-bit sum and product register, and hardware framework for space vector pulse width modulation (SVPWM) application. This DSP was chosen because, in addition to the boost converter control, the pumping system performs a fuzzy MPPT of the photovoltaic panels, the SVPWM drive of the variable frequency inverter, the reading and digital filtering of several analog signals and the general supervision of these processes.

It is important to mention that it is not necessary to control the input current of the converter, since the maximum current supplied by the photovoltaic modules is 18A, while the input fuse of the boost converter is 30A. In addition, the voltage control reference input is done in a 2 second ramp.

(a) Photovoltaic panels.

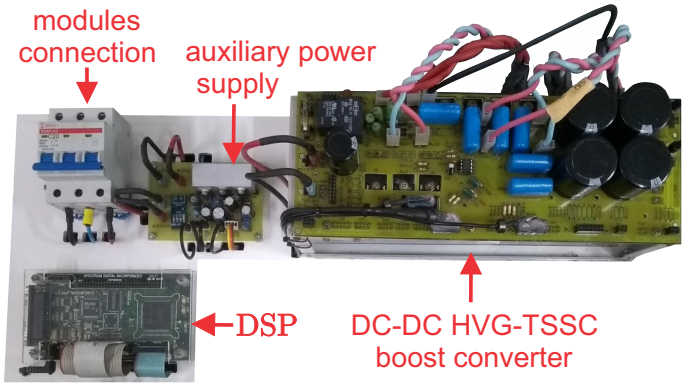

(b) Electronic system.

Figure 1: Full boost converter control system.

3 DC-DC HVG-TSSC BOOST CONVERTER

The DC-DC boost converter used in this work uses the design performed by Silveira *et al.* [6], whose transformer has two secondary windings with ratios equal to 1. The nominal power of the converter is *1 kW*. The authors do not recommend the use of this converter in open loop (without voltage control) and without a load connected to the output, as the output voltage tends to increase to the point of damaging the output capacitors. In addition, the two PWM signals must have a switching frequency of $25\,kHz$ and a phase shift of $180°$. The boost converter diagram is shown in Figure 2.

Since the discontinuous conduction mode of this converter has a response with high nonlinearity [12], a simulation is performed in PSIM® to obtain a small signal model. The specifications of the converter components are described in Table 1. A duty cycle change from 7% to 34% is performed, load R of $30\,k\Omega$ and fixed input voltage of $65\,V$. Using maximum overshoot and settling time information, a second order linear model in the frequency domain can be obtained. Thus, a small-signal model that relates the output voltage of the DC-DC boost converter to the applied duty cycle is estimated according to the following transfer function:

$$G(z) = \frac{V_{cc}(z)}{D(z)} = \frac{0{,}01233z + 0{,}0118}{z^2 - 1{,}858z + 0{,}8728} + 262{,}23\,. \tag{1}$$

The comparison between the response of the estimated model and the simulated boost converter to the mentioned step variation is illustrated in Figure 3. Note that built model does not entirely correspond to the real system response. This is due to the nonlinear nature of the plant. However, there is a good approximation for the settling time and maximum overshoot.

A closed-loop response simulation is performed using the PI controller designed by Ferreira Filho *et al.* [4] for continuous conduction mode, as shown in Figure 4, where $Ref[k]$ is the discrete reference setpoint, $Sens[k]$ is the discrete output signal of the voltage sensor and $e[k] = Ref[k] - Sens[k]$. The sensor gain is defined as $K_s = 0.007395$. Figure 5a shows the response for a small variation of the controller reference (the same variation of the converter output voltage for the small signal test in Figure 3). Although the response has an excellent result for a small reference variation, with a settling time of $2.86\,s$ and zero overshoot, the same does not happen for large reference variations, as illustrated in Figure 5b. The response has $18.7\,\%$ overshoot and a settling time of $19\,s$. These large voltage fluctuations are undesirable for the system of interest.

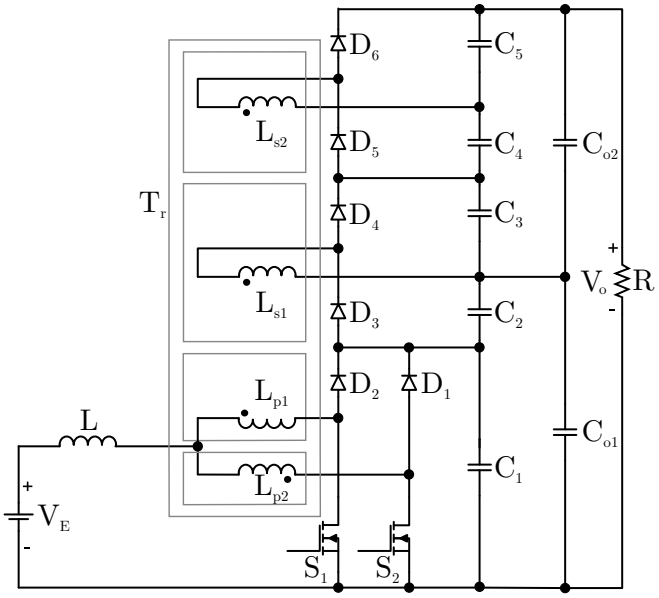

Figure 2: Diagram of the DC-DC HVG-TSSC boost converter.

component	specification	internal resistance
D_1 and D_2	$1.7\,V$ threshold	$0.1\,\Omega$
D_3,D_4, D_5 and D_6	$1.3\,V$ threshold	
S_1 and S_2	$1.3\,V$ drop	$0.021\,\Omega$
L	$60\,\mu H$	$0.001\,\Omega$
$C_1 ... C_5$	$2.2\mu F$	$0.02\,\Omega$
C_{o1} and C_{o2}	$470\,\mu F$	$0.230\,\Omega$

Table 1: Component specifications.

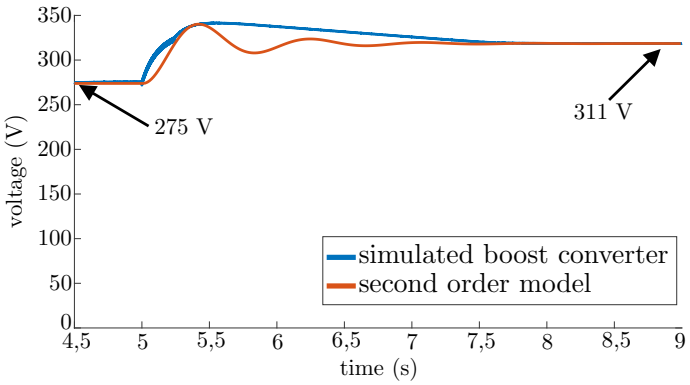

Figure 3: Boost converter responses to a duty cycle step.

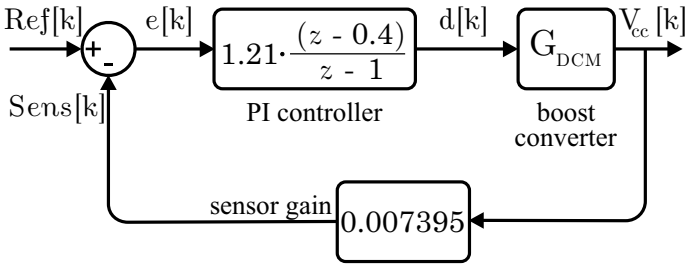

Figure 4: PI control block diagram developed by Ferreira Filho *et al.* [4].

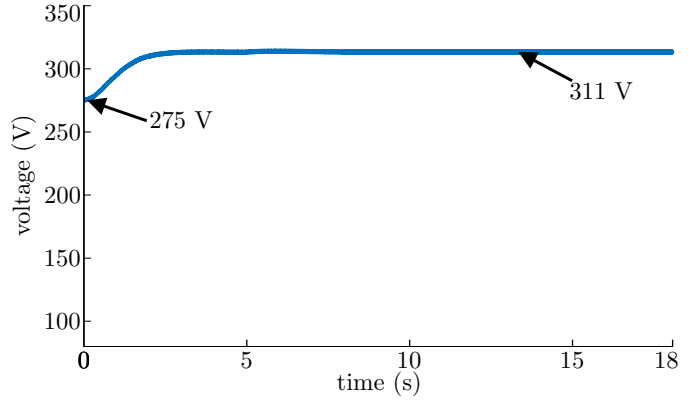

(a) Small controller reference variation.

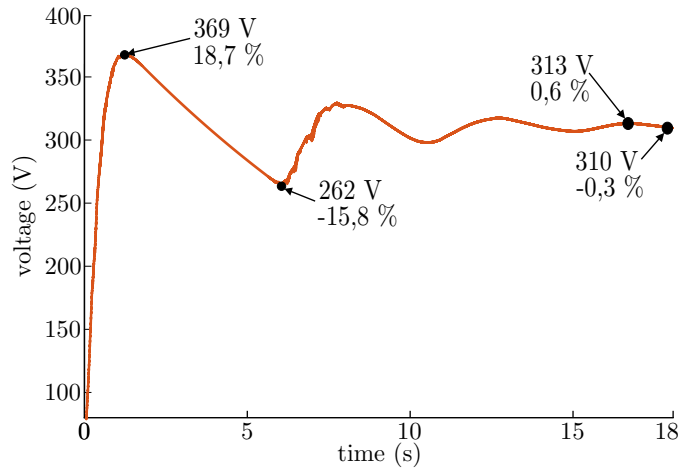

(b) Large controller reference variation.

Figure 5: Simulated boost converter responses to the PI controller.

Analyzing the root locus graph for the Eq. (1) model and Ferreira Filho's PI controller *et al.* [4] shown in Figure 6a, it is observed that most of the root locus is in the region of instability, that is, outside the unit circle. It can also be seen that the complex conjugate poles are dominant, resulting in a theoretical overshoot of $15.6\,\%$. Since the application is powering a DC bus for a photovoltaic pumping system, it is desired a zero overshoot without oscillations. Thus, the PI controller does not meet the project requirements.

The application of a Proportinal Integral Derivative (PID) controller whose root locus is illustrated in Figure 6b also did not produce good results. Among the many possibilities of zeros of the controller, the choice of zeros in 0.8 and 0.9 makes it possible to have points in the roots locus where it is possible to obtain an overshoot of $9.16\,\%$ and dominant real pole. However, a gain of 2280 is required, which makes the controller implementation impossible. Instead of trying to apply other classical controllers such as phase lead and lag, the authors have decided to apply different approaches, such as state feedback controller and fuzzy controller. Since the system has nonlinear behavior for the DCM condition, the use of these controllers are very attractive.

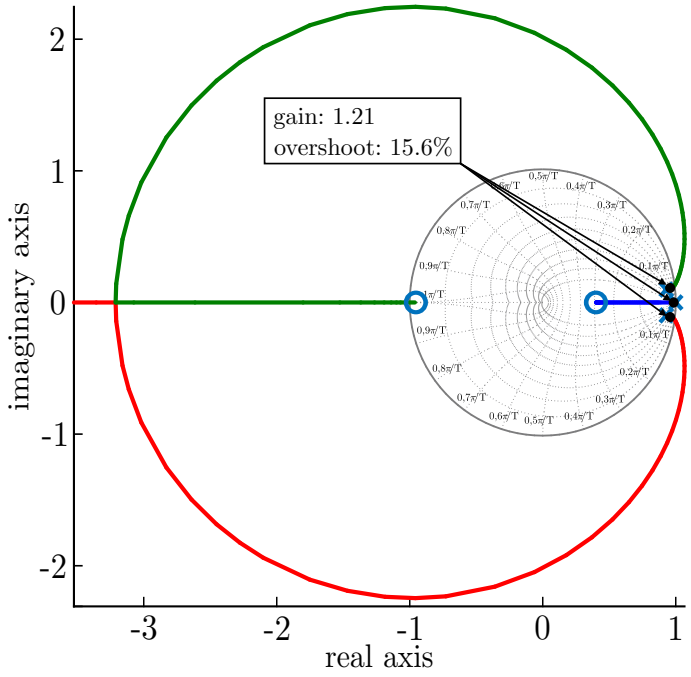

(a) PI controller with zero at 0.4.

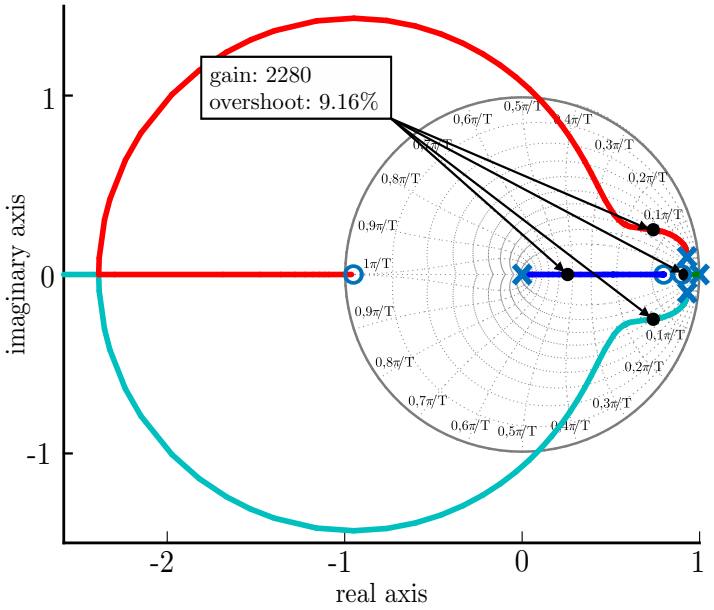

(b) PID controller with zeros at 0.8 and 0.9.

Figure 6: Roots locus for classic digital control.

4 STATE FEEDBACK CONTROLLER

The representation of a discrete time dynamical system by state equations is expressed as

$$\boldsymbol{x}[k+1] = \boldsymbol{A}\boldsymbol{x}[k] + \boldsymbol{B}\boldsymbol{u}[k] \tag{2}$$

and

$$\boldsymbol{y}[k] = \boldsymbol{C}\boldsymbol{x}[k] + \boldsymbol{D}\boldsymbol{u}[k]\,, \tag{3}$$

where $\boldsymbol{x}[k]$ is the states vector, $\boldsymbol{u}[k]$ is the system inputs vector, $\boldsymbol{A}, \boldsymbol{B}, \boldsymbol{C}$ and $\boldsymbol{D}$ are resulting matrices from the system modeling.

The development of Eq. (1) shows that the system has two states. The state equations were calculated from the transfer function present in Eq. (1) so that the states are physical variables of the system, making the implementation of the modern control system easier. For the developed model, the states $x_1[k]$ and $x_2[k]$ are respectively $y[k]$ and $y[k-1]$, that is, the current and previous output of the system. Also, the system input $\boldsymbol{u}[k]$ is the duty cycle $d[k]$.

A modern control system is designed by state feedback with integral action via pole placement. The block diagram is illustrated in Figure 7, where

$$v[k] = v[k-1] + e[k] \tag{4}$$

$$d[k] = K_i v[k] - \boldsymbol{K_x}\boldsymbol{x}[k]\,. \tag{5}$$

The gains K_i and $\boldsymbol{K_x}$ are the integrator gain and the state gain vector, respectively. Allocating the poles at 0.8, the gains obtained are $K_i = 0.297$ and $\boldsymbol{K_x} = [25,592 \quad -21,245]$. More information about these gains calculations can be found at Ogata *et al.* [13].

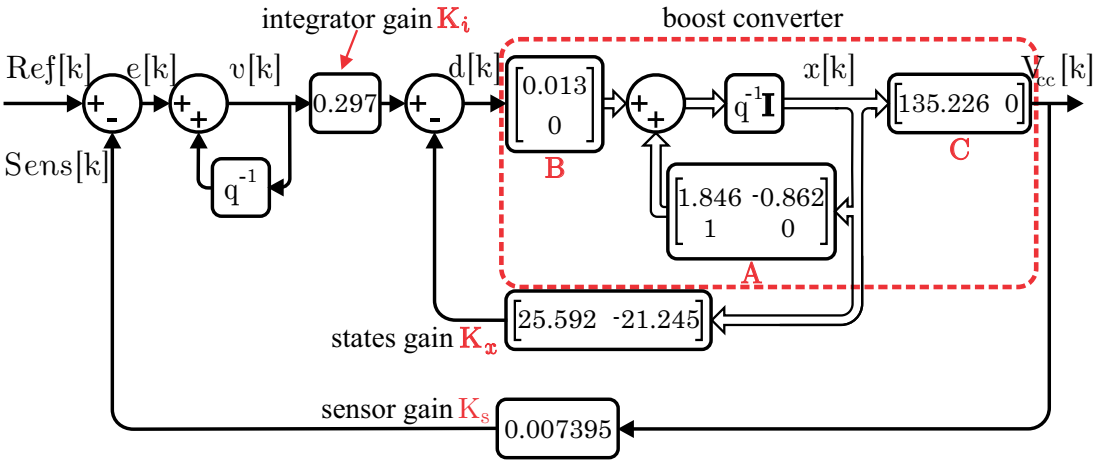

Figure 7: State feedback control block diagram.

5 FUZZY CONTROLLER DESIGN

Among the classic types of fuzzy controllers, the Takagi-Sugeno [14] controller and the Mamdani controller [15] stands out. In this work, the Mamdani-type controller is used. The structure of this type of fuzzy inference system is illustrated in Figure 8, while the block diagram of the fuzzy control system is shown in Figure 9. According to Perry *et al.* [16], the inputs used in a fuzzy control system where the steady state error is desired to be zero are usually the error between the desired value and the system output ($e[k]$) and its variation ($\Delta e[k]$), defined as

$$\Delta e[k] = e[k] - e[k-1]\,. \tag{6}$$

The controller output is the duty cycle variation $\Delta d[k]$, and the update of $d[k]$ should be performed as follows:

$$d[k] = d[k-1] + \Delta d[k]\,. \tag{7}$$

Figure 8 shows a fuzzy representation for the numerical input values. This is obtained through the membership functions (MFs) associated with each fuzzy set in the input space. For each input value, membership degrees are assigned (μ) according to the defined fuzzy sets. The MFs can have different shapes such as triangular, trapezoidal and gaussian. However, its range must be from 0 to 1 to normalize the inputs [17].

Five membership functions are chosen for the universe of discourse of each fuzzy input and output, having triangular and trapezoidal shapes: Negative Big (NB), Negative Small (NS), Zero (ZE), Positive Small (PS) and Positive Big (PB). After a tuning process, the input and output MFs of the fuzzy system are chosen, as illustrated in Figure 10. It is important to mention that the shapes of membership functions were chosen by the authors according to their knowledge about the system. As can

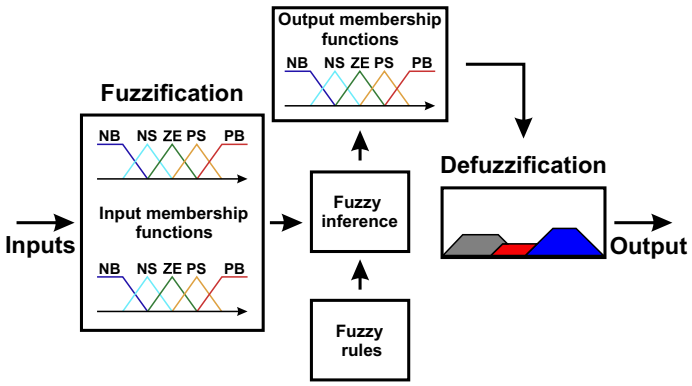

Figure 8: Structure of a fuzzy inference system.

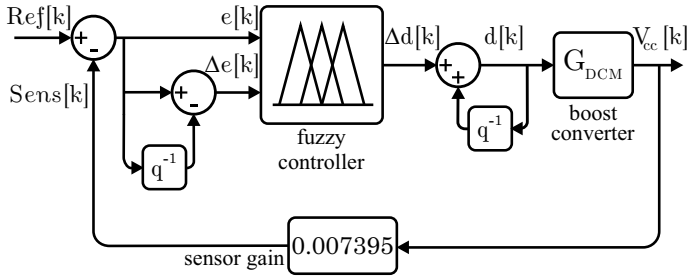

Figure 9: Block diagram of the fuzzy control system.

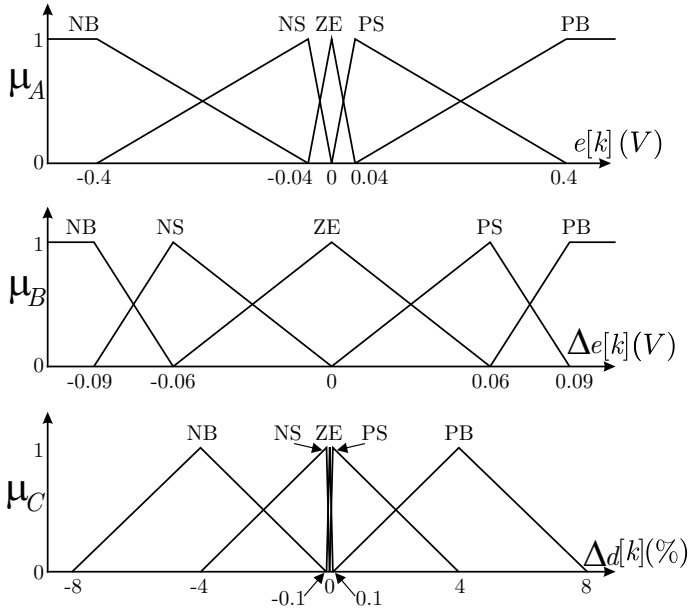

Figure 10: Universe of discourse's MFs of fuzzy variables.

be inferred from Figure, the membership functions NB and PB saturate both at 1 for large positive/negative values of $\Delta e[k]$ at the extremes of the universe of discourse's input. This means that values of $\Delta e[k]$ either below -0.09 or larger than 0.09 may occur and are considered large in magnitude. In the universe of discourse's output, the membership functions NB and PB are triangular. This means that values of $\Delta d[k]$ should be kept around the range between -4 and +4. Values of $\Delta d[k]$ in the range (-8, -4) and (+4, +8) are possible to occur, but less probable because they are weighted by the decreasing portions of the membership functions NB and PB, respectively. Values of $\Delta d[k]$ either lower than -8 or larger than +8 are not allowed at all.

As there is an overlap between the membership functions, two MFs may be activated for the same input, each each one with its respective membership degree μ. In general, for a two-input system, four membership functions are activated.

In the inference step, the fuzzified inputs are mapped to the fuzzy rules, producing a fuzzy output for each rule. The degree of membership of the output is determined by the degrees of membership of the inputs from a mathematical implication, such as that of Zadeh, Mamdami, Larsen or Lukasiewicz [18]. The activation of the i-th rule, μ_{Ci}, in this work is obtained from the MFs

inputs membership degrees $\mu_A(e)$ and $\mu_B(\Delta e)$, using Larsen's operator, as

$$\mu_{C_i}\left(e[k], \Delta e[k]\right) = \mu_{A_i}(e[k]) \cdot \mu_{B_i}(\Delta e[k])\,, \tag{8}$$

where $A_i, B_i \in \{\text{NB,NS,ZE,PS,PB}\}$ are the fuzzy sets of the input variables $e[k]$ and $\Delta e[k]$, respectively.

The 25 fuzzy rules were obtained with IF-THEN statements from the analysis of the boost converter response to the classic PI controller (see Figure 5) as shown in Figure 11. The red numbers represent some of the generated rules, whose complete set is presented in Table 2 and compactly illustrated in Figure 12. In this figure, there are evidences of smooth transitions between the membership functions in the universe of output discourse. In this work, we use the product rule as the implication operator. Thus, the fuzzy set in the consequent of the i-th rule is modified by the activation of this rule as follows:

$$C_i^*(\Delta d) = \mu_{C_i}(e[k], \Delta e[k]) \cdot C_i(\Delta d[k])\,, \tag{9}$$

whose effect on the output fuzzy set of the i-th rule is illustrated in Figure 13.

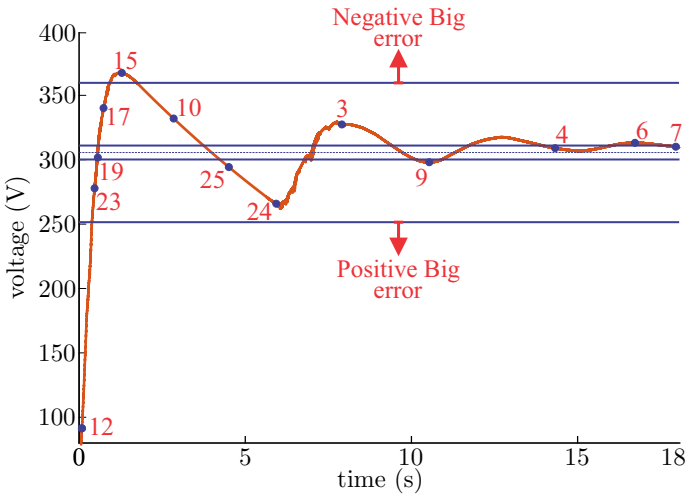

Figure 11: Conception of fuzzy rules.

Rule	If	$e[k]$	and	$\Delta e[k]$	Then	Output	Rule	If	$e[k]$	and	$\Delta e[k]$	Then	Output
1		NB		PS		NB	13		NB		NB		NB
2	IF	PB	AND	NB	THEN	ZE	14	IF	NB	AND	NS	THEN	NB
3		NS		ZE		NB	15		NB		ZE		NB
4		NS		PS		NS	16		NS		NB		NB
5		NS		PB		ZE	17		NS		NS		NB
6	IF	ZE	AND	ZE	THEN	ZE	18	IF	ZE	AND	NB	THEN	NB
7		ZE		PS		ZE	19		ZE		NS		NB
8		ZE		PB		PS	20		PS		NB		NB
9		PS		ZE		ZE	21		PS		NS		NS
10		PS		PS		ZE	22		NB		PB		NB
11	IF	PS	AND	PB	THEN	PS	23	IF	PB	AND	NS	THEN	ZE
12		PB		PB		PB	24		PB		ZE		PS
							25		PB		PS		PS

Table 2: Fuzzy rules of the proposed voltage control.

$\Delta e[k]$ \ $e[k]$	NB	NS	ZE	PS	PB
NB	NB	NB	NB	NB	ZE
NS	NB	NB	NB	NS	ZE
ZE	NB	NB	ZE	ZE	PS
PS	NB	NS	ZE	ZE	PS
PB	NB	ZE	PS	PS	PB

Figure 12: Simplified fuzzy rules.

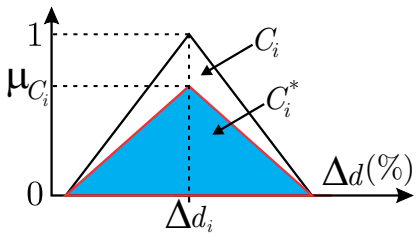

Figure 13: Example of the effect of the product rule used as the implication operator on the output fuzzy set of the i-th rule.

Finally, the last step of a fuzzy controller is the defuzzification. The task of the defuzzification process is to convert the fuzzy rules output into a scalar value to be applied to the control process [17]. There are several methods for finding an approximate scalar value to represent the action to be taken such as the max-min method, the average method and the centroid method. The defuzzification method used in this work is the Weighted Triangular Median Average, a variation of Weighted Trapezoid Median Average method described in [19] as

$$\Delta d[k] = \frac{\sum_{i=1}^{4} \Delta d_i \, Area_i}{\sum_{i=1}^{4} Area_i}, \tag{10}$$

where Δd_i is the output value associated with the maximum of the modified output fuzzy set of the i-th rule and $Area_i$ is the area of MF C_i^*, as shown in Figure 13 in blue.

6 RESULTS AND DISCUSSION

The simulation results of applying the fuzzy controller to the system compared with the classic PI controller and state feedback controller with integral action are reported in Figure 14 and in Table 3. The controllers sample time is $16\,ms$. It can be seen that there is an overshoot of $0.5\,\%$ in the system response to the fuzzy controller, compared to 18.7% with the classic PI controller and $2.3\,\%$ with the state feedback controller.

The $0.5\,\%$ overshoot of the fuzzy controller is considered insignificant for the design specifications. It is also noted that there are no oscillations like the PI response. In addition to the smaller overshoot, the system response to the fuzzy controller also has a shorter settling time. In fact, the settling time with the fuzzy controller is $1.1\,s$, while for the PI controller it is $19\,s$ and $8\,s$ for the state feedback controller. As already mentioned, the large voltage fluctuations present in the response with the PI controller

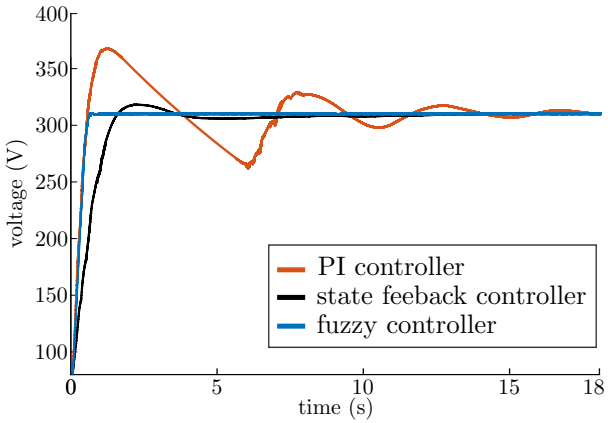

(a) Controlled output voltage.

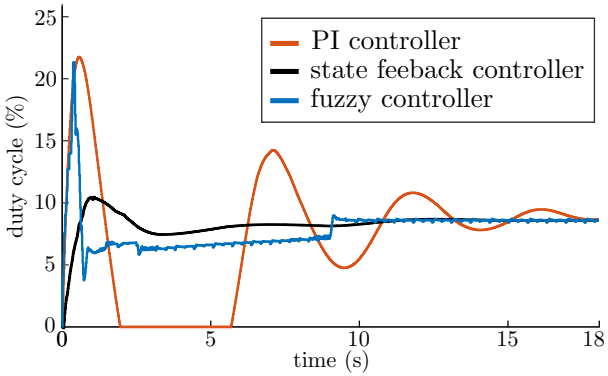

(b) Controllers output.

Figure 14: Simulated system responses with controllers.

controller	overshoot	undershoot	settling time
classic PI	$18.7\,\%$ ($369\,V$)	$-15.8\,\%$ ($262\,V$)	$19\,s$
state feedback	$2.3\,\%$ ($318.2\,V$)	$-1.6\,\%$ ($306.1\,V$)	$8\,s$
fuzzy	$0.5\,\%$ ($311.7\,V$)	$-0.2\,\%$ ($310.4\,V$)	$1.1\,s$

Table 3: Metrics of the simulated system responses.

are undesirable for this photovoltaic pumping system. The fuzzy controller also performs better than the PI controller and state feedback controller in this requirement.

The outputs of the simulated controllers (duty cycle) are illustrated in Figure 14b. It can be seen that during a period of $3.75\,s$, the output of the PI controller is saturated at $0\,\%$, exhibiting undesirable behavior. Large oscillations are also noted. A small oscillation can be observed in the control output by state feedback, responsible for the $2.3\,\%$ overshoot and for a longer settling time. By its turn, although there is a rapid oscillation in the fuzzy controller response, the boost converter response has no overshoot and has a short settling time.

The activation path of fuzzy controller is illustrated in Figure 15. It is noted that there is a convergence in the trajectory of activations, an evidence of system stability. However, not all rules are used. In fact, only 12 of the 25 rules are active. These activated rules are displayed on the left side of Table 2, numbered from 1 to 12. The authors do not consider it prudent to remove the other 13 rules since, during the system's operation in a real scenario, these rules may be activated as a consequence of the increase and/or reduction of solar irradiance on the panels, and parametric changes in the system, such as increased dirtiness or aging of the photovoltaic modules, increased friction in the motor-pump set, etc.

The results of the implementations of fuzzy and classic PI controllers (the best and worst results in Figure 14 and Table 3) in the real system of Figure 1 are presented in Figure 16 and Table 4. The photovoltaic pumping system is started and a frequency (speed) ramp is performed to drive the motor connected to the pump. The output power of the photovoltaic pumping system is proportional to the cube of the pump speed. This output power is reflected to the boost converter and the photovoltaic panels. Thus, for a speed ramp, the DC-DC HVG-TSSC boost converter load input is parabolic.

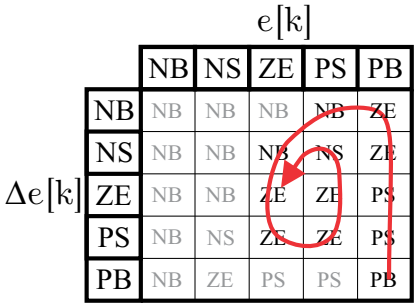

Figure 15: Trajectory of controller rule activations.

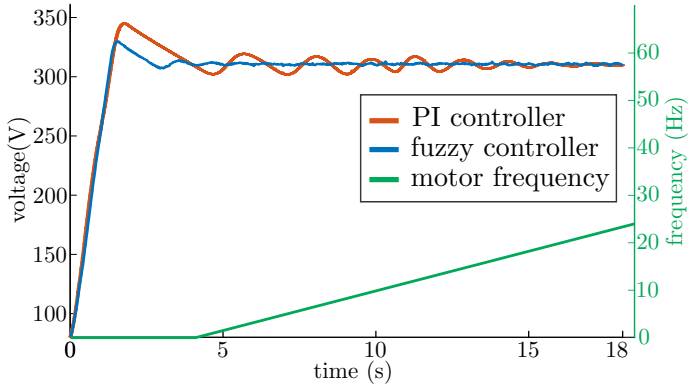

Figure 16: Real system responses to controllers.

controller	overshoot	undershoot	settling time
classic PI	$11.2\,\%$ ($346\,V$)	-2.57% ($303\,V$)	$16\,s$
fuzzy	$5.78\,\%$ ($329\,V$)	-1.6% ($306\,V$)	$3.8\,s$

Table 4: Metrics of the real system responses.

It can be seen that in the real system with a fuzzy controller, although there is an overshoot of 5.78%, which corresponds to a $329\,V$ peak, it quickly vanishes and the transient period lasts only $3.8\,s$, without large oscillations. In the real system with PI controller, the overshoot is 11.2%, with a peak of $346\,V$. The transient period is 16 seconds with large oscillations.

The classic PI controller to DC-DC HVG-TSSC boost converter in DCM turned out to be inadequate, making it impossible for the MPPT algorithm of photovoltaic panels to perform well, as can be seen in Figure 17a. It is noted that the power of the photovoltaic panels in response to the motor speed ramp for a constant irradiance has large oscillations at its beginning. As mentioned, this happens due to voltage oscillations caused by the classical PI controller in the DCM region.

It is noticed that the oscillations stop only when the DC-DC HVG-TSSC boost converter switches to continuous conduction mode. This happens because the classic PI controller was designed to work in this conduction mode. Using two controllers, the classic PI and fuzzy, to control the DC-DC HVG-TSSC boost converter in the discontinuous and continuous conduction regions, respectively, it is noticed that the power of the panels stops oscillating, allowing the application of an MPPT algorithm, as can be seen in Figure 17b. Experimental observations show that, from the commanded frequency on the motor of 24 Hz, there are no more oscillations. The power curves have slightly different final values due to different constant values of irradiance on the panels at the time of acquisition.

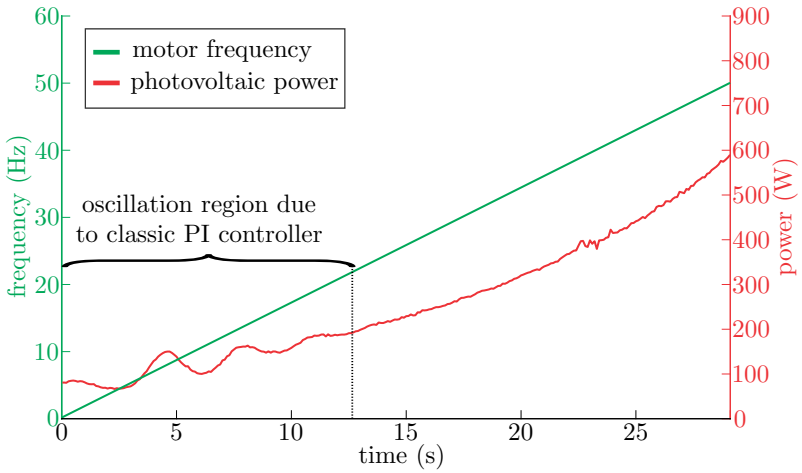

(a) Classic PI controller.

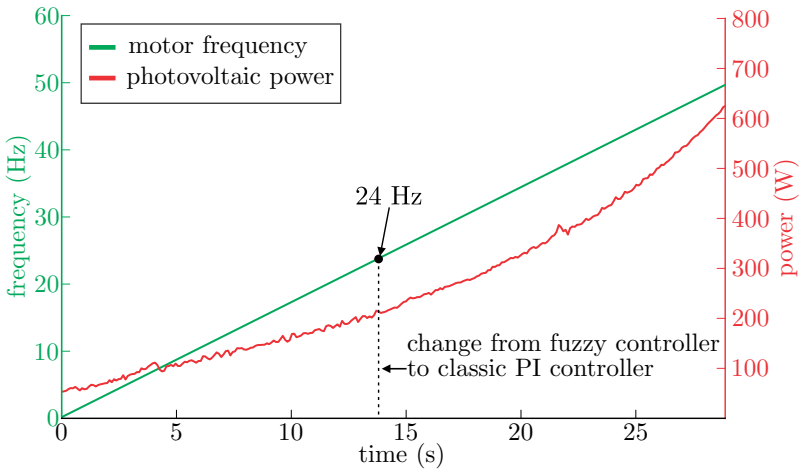

(b) PI classic and fuzzy controllers.

Figure 17: Power of the photovoltaic panels to the motor frequency ramp.

7 CONCLUSIONS

The use of a conventional controller for the DC-DC HVG-TSSC boost converter in DCM causes large fluctuations in the DC link voltage of the pumping system (see Figure 16). These oscillations are reflected to the panels, and can negatively affect the functioning of an MPPT algorithm (see Figure 17a). The use of the fuzzy controller for the DCM region substantially reduced the amplitude and duration of the DC bus voltage oscillations. Without this change in controller, the large power oscillations of the panels could make it impossible for an MPPT to work correctly in the pumping system.

It is important to mention that other fuzzy controllers for classic boost converters in continuous conduction mode should not be used in the DC-DC HVG-TSSC boost converter because they have different topologies, and mainly because, in this specific case, they work in different conduction modes.

The fuzzy control output has no oscillations like the PI controller and the state feedback controller and there is no saturation. The fuzzy rules trajectory evidences that the system is stable. The real response of the fuzzy controller system has an overshoot of $5.78\,\%$ ($329\,V$) and settling time of $3.8\,s$. The practical implementation of this fuzzy controller in the DSP device with all 25 rules did not present any operational or processing problems. For this pumping system with MPPT, the fuzzy voltage controller of the DC-DC HVG-TSSC boost converter proved to be satisfactory for the discontinuous conduction mode, considering the requirements of the real application.

8 ACKNOWLEDGEMENTS

The present work was carried out with the support of CAPES (Funding Code 001) and CNPq (No. 309379/2019-9).

REFERENCES

[1] A. Raju, S. R. Kanik and R. Jyoti. "Maximum efficiency operation of a single stage inverter fed induction motor PV water pumping system". In *2008 First International Conference on Emerging Trends in Engineering and Technology*, pp. 905–910, 2008.

[2] V. Vongmanee. "The photovoltaic pumping system using a variable speed single phase induction motor drive controlled by field oriented principle". In *The 2004 IEEE Asia-Pacific Conference on Circuits and Systems, 2004. Proceedings.*, volume 2, pp. 1185–1188, 2004.

[3] R.-J. Wai, C.-Y. Lin, R.-Y. Duan and Y.-R. Chang. "High-efficiency DC-DC converter with high voltage gain and reduced switch stress". *IEEE Transactions on Industrial Electronics*, vol. 54, no. 1, pp. 354–364, 2007.

[4] J. R. M. Ferreira Filho, F. R. F. Mendes, I. R. Sousa, J. R. B. Sousa and C. M. S. Medeiros. "Photovoltaic Panel Based Pumping System: A Solution Without Batteries". *IEEE Latin America Transactions*, vol. 16, no. 2, pp. 514–520, 2018.

[5] G. V. Torrico-Bascopé, S. A. Vasconcelos, R. P. Torrico-bascope, F. L. Antunes, D. S. De Oliveira and C. G. Branco. "A high step-up DC-DC converter based on three-state switching cell". In *2006 IEEE International Symposium on Industrial Electronics*, volume 2, pp. 998–1003, 2006.

[6] G. C. Silveira, F. L. Tofoli, L. D. S. Bezerra and R. P. Torrico-Bascopé. "A nonisolated DC-DC boost converter with high voltage gain and balanced output voltage". *IEEE Transactions on Industrial Electronics*, vol. 61, no. 12, pp. 6739–6746, 2014.

[7] A. Mamizadeh, N. Genc and R. Rajabioun. "Optimal tuning of PI controller for boost DC-DC converters based on cuckoo optimization algorithm". In *2018 7th international conference on renewable energy research and applications (ICRERA)*, pp. 677–680. IEEE, 2018.

[8] J. C. Mayo-Maldonado, J. C. Rosas-Caro, R. Salas-Cabrera, A. González-Rodriguez, O. F. Ruíz-Martínez, R. Castillo-Gutiérrez, J. R. Castillo-Ibarra and H. Cisneros-Villegas. "State space modeling and control of the DC-DC multilevel boost converter". In *2010 20th International Conference on Electronics Communications and Computers (CONIELECOMP)*, pp. 232–236, 2010.

[9] M. Leng, G. Zhou, Q. Tian, G. Xu and F. Blaabjerg. "Small Signal Modeling and Design Analysis for Boost Converter With Valley V^2 Control". *IEEE Transactions on Power Electronics*, vol. 35, no. 12, pp. 13475–13487, 2020.

[10] K. Eltag, M. S. Aslamx and R. Ullah. "Dynamic stability enhancement using fuzzy PID control technology for power system". *International Journal of Control, Automation and Systems*, vol. 17, no. 1, pp. 234–242, 2019.

[11] N. N. Ismail, I. Musirin, R. Baharom and D. Johari. "Fuzzy logic controller on DC/DC boost converter". In *2010 IEEE International Conference on Power and Energy*, pp. 661–666. IEEE, 2010.

[12] I. R. Sousa. "Sistema de bombeamento fotovoltaico com conversores eletrônicos integrados." Master's thesis, Instituto Federal de Educação, Ciência e Tecnologia do Ceará, 2020.

[13] K. Ogata *et al.*. *Modern control engineering*, volume 5. Prentice hall Upper Saddle River, NJ, 2010.

[14] T. Takagi and M. Sugeno. "Fuzzy identification of systems and its applications to modeling and control". *IEEE transactions on systems, man, and cybernetics*, , no. 1, pp. 116–132, 1985.

[15] E. H. Mamdani and S. Assilian. "An experiment in linguistic synthesis with a fuzzy logic controller". *International journal of man-machine studies*, vol. 7, no. 1, pp. 1–13, 1975.

[16] A. G. Perry, G. Feng, Y.-F. Liu and P. C. Sen. "A design method for PI-like fuzzy logic controllers for DC-DC converter". *IEEE transactions on industrial electronics*, vol. 54, no. 5, pp. 2688–2696, 2007.

[17] A. P. Engelbrecht. *Computational intelligence: an introduction*. John Wiley & Sons, 2007.

[18] H. B. Verbruggen, H.-J. Zimmermann and R. Babuška. *Fuzzy algorithms for control*, volume 14. Springer Science & Business Media, 2013.

[19] H. R. Mahdiani, A. Banaiyan, M. H. S. Javadi, S. M. Fakhraie and C. Lucas. "Defuzzification block: New algorithms, and efficient hardware and software implementation issues". *Engineering Applications of Artificial Intelligence*, vol. 26, no. 1, pp. 162–172, 2013.